Chinese Chemical Letters 37 (2026) 110667

Contents lists available at ScienceDirect

Chinese Chemical Letters

journal homepage: www.elsevier.com/locate/cclet

Regulatory effects of coronene and pyridine on the self-assembly structure of tetracarboxylic acid derivative formed by dimeric building blocks

Linlin Gan[a,1], Xuan Peng[c,1], Wenchao Zhai[c], Cheng Zhang[d], Xinyu Duan[c], Ke Deng[a,*], Wei Li[c,*], Qingdao Zeng[a,b,*]

[a] CAS key Laboratory of Standardization and Measurement for Nanotechnology, CAS Center for Excellence in Nanoscience, National Center for Nanoscience and Technology (NCNST), Beijing 100190, China
[b] Center of Materials Science and Optoelectronics Engineering, University of Chinese Academy of Sciences, Beijing 100049, China
[c] School of Science, Nanchang Institute of Technology, Nanchang 330099, China
[d] School of Materials Science and Engineering, South China University of Technology, Guangzhou 510641, China

ARTICLE INFO

Article history:
Received 25 September 2024
Revised 7 November 2024
Accepted 21 November 2024
Available online 23 November 2024

Keywords:
Regulation
Co-assembly
Hydrogen bond
Pyridine
STM

ABSTRACT

The regulation of guest molecules on the self-assembly system of tetracarboxylic acid derivative (H_4BDETP) at the liquid/solid interface was studied by scanning tunneling microscopy (STM) and density functional theory (DFT) calculations. Coronene (COR) guest molecules induced H_4BDETP to transform from linear assembly structure to diversified nanoporous structures in which COR could be captured. And the regulation of pyridine guest molecules (DPE, BPYB, TYPY) on the mono-component assembly structure of H_4BDETP was achieved by forming O–H···N hydrogen bonds with H_4BDETP. The introduction of both COR and pyridine derivatives could destroy the hydrogen-bonded dimers of H_4BDETP, and new O–H···O hydrogen bonds were formed between H_4BDETP molecules. In addition, H_4BDETP/pyridine co-assembly structures depended on the central bridging units and the number of pyridine groups in pyridine derivatives. Furthermore, H_4BDETP/TYPY structure underwent structural transformation induced by COR and multi-component assembly structures with thermodynamic stability were constructed.

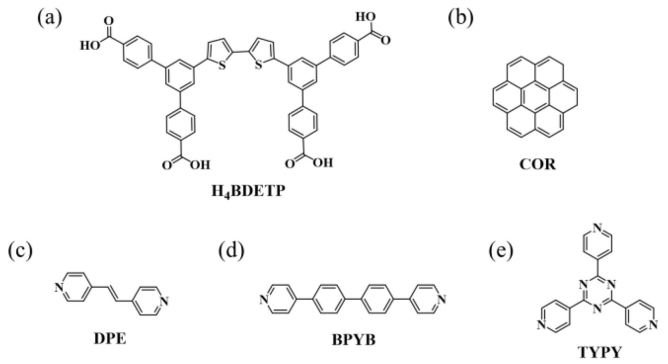
© 2025 Published by Elsevier B.V. on behalf of Chinese Chemical Society and Institute of Materia Medica, Chinese Academy of Medical Sciences.

Supramolecular self-assembly has been widely applied in the preparation of diverse functional nanomaterials with specific nanostructures spontaneously formed by building blocks through intermolecular non-covalent bonds [1–3]. Recently, researches on two-dimensional supramolecular self-assembly studied by scanning tunneling microscopy (STM) have gained considerable attention, which helps to intuitively reveal intermolecular interaction modes and explore the laws of supramolecular self-assembly [4–7]. Currently, the fabrication of host-guest systems has received much concern, as it is an effective approach to achieve specific distribution of heterogeneous molecules and prepare various composite assembly structures [8–11]. Due to the selectivity and directionality of hydrogen bonds, the self-assembly nanostructures driven by hydrogen bonds are more predictable when compared with other non-covalent bonds. And this makes the self-assembly structures of aromatic acid derivatives widely used as host structures in host-guest systems [12–16]. Two-dimensional assembly structures are the result of the intermolecular interactions, molecule-solvent interactions, and molecule-substrate interactions [17]. And in the bi-component or multi-component systems, more types of molecules are involved, so further researches are needed for the controllable preparation of bi-component and multi-component structures.

In the previous reports, it is found that pyridine derivatives can break the original O–H···O hydrogen bonds between aromatic acid derivatives and form stronger O–H···N hydrogen bonds with aromatic acid derivatives, which can regulate the self-assembly structures of aromatic acid derivatives and show broad application prospects in the fabrication of abundant binary nanostructures [18–25]. But few researches about the pyridine regulation of dimeric building blocks formed by hydrogen bonds between aromatic acid molecules have been reported. For instance, the introduced pyridine derivatives could regulate the self-assembly structure aggregated by 5′-(4-carboxyphenyl)-[1,1′:3′,1″-terphenyl]-3,3″,5,5″-tetracarboxylic acid (H_5BHB) dimer building blocks, while H_5BHB still appeared as

* Corresponding authors.
E-mail addresses: kdeng@nanoctr.cn (K. Deng), liweidting@nit.edu.cn (W. Li), zengqd@nanoctr.cn (Q. Zeng).
[1] These authors contributed equally to this work.

https://doi.org/10.1016/j.cclet.2024.110667
1001-8417/© 2025 Published by Elsevier B.V. on behalf of Chinese Chemical Society and Institute of Materia Medica, Chinese Academy of Medical Sciences.



Scheme 1. Chemical structures of H_4BDETP, COR and pyridine derivatives including DPE, BPYB and TYPY.

dimer in its bi-component systems with pyridine derivatives [26]. For 5′-(4,5-bis(4-carboxyphenyl)-2,5-dihydro-1*H*-imidazole-2-yl)-[1,1′:3′,1″-terphenyl]-4,4″-dicarboxylic acid (BCDTDA) molecule containing an imidazole group, BCDTDA molecules self-assembled into ordered structures in the form of dimeric building blocks *via* intermolecular N–H···O hydrogen bonds. Both coronene (COR) and 4,4′-bipyridine (BP) could induce the structural transformation of BCDTDA, but had no effect on the BCDTDA dimers [27]. However, the addition of pyridine derivative with alkoxy chains (PEBP-C4, PEBP-C8) was able to destroy BCDTDA dimers, and multiple co-assembly structures were prepared. In this work, the self-assembly dimeric structure of aromatic carboxyl acid derivative regulated by various guest molecules including pyridine derivatives and COR was investigated. Differently, dimeric building blocks formed by aromatic carboxyl acid could be disrupted by any of these introduced guest molecules.

As shown in Scheme 1, three types of pyridine derivatives and COR were utilized to regulate the self-assembly structure of 5′,5‴′-([2,2′-bithiophene]-5,5′-diyl)bis([1,1′:3′,1″-terphenyl]-4,4″-dicarboxylic acid)) (H_4BDETP) respectively. And pyridine derivatives included (*E*)-1,2-di(pyridin-4-yl)ethene (DPE), 4,4′-di(pyridin-4-yl)-1,1′-biphenyl (BPYB) and 2,4,6-tri(pyridin-4-yl)-1,3,5-triazine (TYPY). COR was introduced into H_4BDETP/TYPY co-assembly system to fabricate multi-component structure. Combined with STM experimental results and DFT calculations, the formation mechanisms of these co-assembly structures were studied, which might be helpful for deepening insight into the formation of co-assembly structures.

H_4BDETP molecules formed dimeric building blocks *via* two pairs of hydrogen bonds between carboxyl groups and self-assembled into linear structure at 1-heptanoic acid/HOPG interface as previously reported [28]. The introduced COR induced the structural transformation of H_4BDETP's self-assembly system, and three types of H_4BDETP/COR co-assembly structures were obtained in Fig. S1 (Supporting information). Figs. 1a–c were their high-resolution STM images and provided more details. The adsorption conformation of H_4BDETP was changed by adding COR molecules. In H_4BDETP/COR-I co-assembly structure (Fig. 1a), H_4BDETP molecules appeared as H-shaped bright spots, and each COR molecule appearing as circular bright spot was captured by the cavity formed by four H_4BDETP molecules. Minor difference existed in the tilt angle of H_4BDETP molecules between adjacent rows. A unit cell was depicted in Fig. 1a and its experimental parameters for H_4BDETP/COR-I structure (Table S1 in Supporting information) were: $a = 3.3 \pm 0.1$ nm, $b = 4.2 \pm 0.1$ nm, $\alpha = 90° \pm 1°$. The ratio of H_4BDETP to COR was 1:1. Based on STM experimental results, the optimized assembly model for H_4BDETP/COR-I structure was built by DFT calculations and presented in Fig. 1d. H_4BDETP dimers disintegrated and all carboxyl groups of each

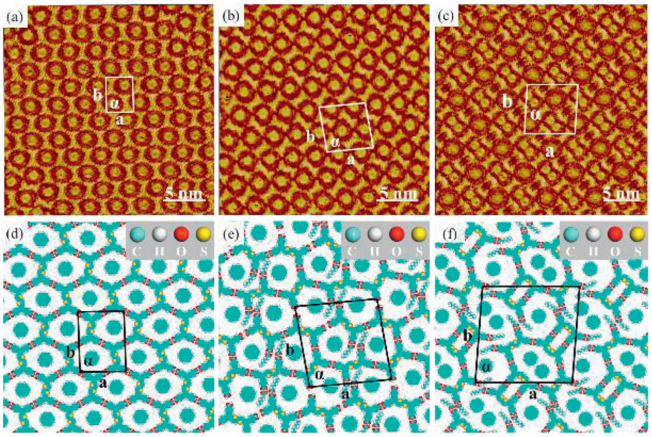


Fig. 1. High-resolution STM images of H_4BDETP/COR co-assembly structures with the scanning conditions of $I_{set} = 375.4$ pA, $V_{bias} = 558.5$ mV: (a) H_4BDETP/COR-I, (b) H_4BDETP/COR-II, (c) H_4BDETP/COR-III. (d-f) Corresponding optimized molecular models for the structures in (a–c) respectively. The insets in (d–f) indicated the blue atom was carbon, the white atom was hydrogen, the red atom was oxygen and the yellow atom was sulfur.

H_4BDETP molecule formed O–H···O hydrogen bonds with those of four H_4BDETP molecules. The calculated lattice parameters for H_4BDETP/COR-I co-assembly structure in Table S1 were consistent with the corresponding experimental lattice parameters, indicating the optimized structural model was reasonable.

In H_4BDETP/COR-II structure (Fig. 1b), each COR molecule was surrounded by four H_4BDETP molecules and the tilt angles of neighboring H_4BDETP molecules in the same row were slightly different, which were similar to the H_4BDETP/COR-I structure. However, the difference between the orientations of H_4BDETP molecules in adjacent rows was significant. The ratio of H_4BDETP to COR was 1:1. And the unit cell parameters for H_4BDETP/COR-II structure were measured to be: $a = 5.5 \pm 0.1$ nm, $b = 5.4 \pm 0.1$ nm, $\alpha = 95° \pm 1°$. As shown in Fig. 1e, all H_4BDETP dimers were destroyed. Two carboxyl groups of H_4BDETP molecule formed O–H···O hydrogen bonds with those of neighboring H_4BDETP molecules in the same row. Along axis *b* direction, one of H_4BDETP's remaining carboxyl groups formed hydrogen bond with H_4BDETP molecule in the neighboring row while the other was exposed on the substrate, or both combined with heptanoic acid to form hydrogen bonds, respectively.

Compared to the above co-assembly structures, H_4BDETP molecules in H_4BDETP/COR-III structure (Fig. 1c) appeared as arch-shaped or H-shaped bright spots, implying that a part of H_4BDETP dimers were kept despite the participation of COR. And H_4BDETP monomers distributed between the adjacent columns of H_4BDETP dimers. Hexagonal and rectangular cavities were formed by H_4BDETP molecules to accommodate one or two COR molecules respectively. The measured lattice parameters for H_4BDETP/COR-III co-assembly structure were: $a = 6.9 \pm 0.1$ nm, $b = 6.9 \pm 0.1$ nm, $\alpha = 86° \pm 1°$. And the ratio of H_4BDETP to COR was 1:1 in the co-assembly structure. The structural model (Fig. 1f) indicated that two H_4BDETP dimers were connected by two H_4BDETP monomers through hydrogen bonds between carboxyl groups, which constituted a rectangular cavity and could be considered as the building block. And the remaining carboxyl groups of each building block combined with those of heptanoic acid molecules.

Total energies including intermolecular interactions and molecules-substrate interactions for H_4BDETP/COR co-assembly structures were given in Table S2 (Supporting information). To better compare the thermodynamic stability of assembly structures, total energy per unit area instead of total energy was employed because of different lattice parameters for the unit cells

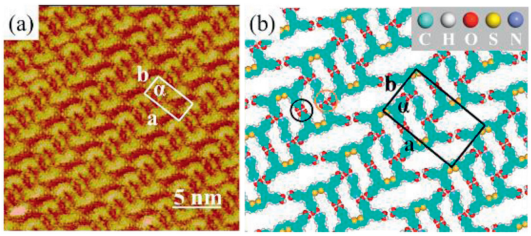


Fig. 2. (a) High-resolution STM image of H_4BDETP/DPE co-assembly structure, the scanning conditions were: $I_{set} = 271.6$ pA, $V_{bias} = 764.8$ mV; $I_{set} = 302.1$ pA, $V_{bias} = 710.4$ mV. (b) The calculated molecular model for H_4BDETP/DPE co-assembly structure. The inset in (b) indicated the blue atom was carbon, the white atom was hydrogen, the red atom was oxygen, the yellow atom was sulfur and the purple atom was nitrogen.

of these assembly structures. Table S2 showed that total energies per unit area of three kinds of H_4BDETP/COR structures were −0.273, −0.273 and −0.281 kcal mol^{-1} Å^{-2}, respectively. They were approximately equal, and this was energetically beneficial for their co-existence on HOPG.

When DPE was added to H_4BDETP's mono-component system, an ordered co-assembly structure similar to H_4BDETP's linear structure was observed (Fig. S2 in Supporting information). It was well distinguished in high-resolution image (Fig. 2a) that arch-shaped and short rod-shaped bright spots corresponded to H_4BDETP and DPE molecules respectively. H_4BDETP molecules distributed in a face-to-face manner were slightly staggered between each other, indicating that DPE molecules have disrupted H_4BDETP dimers. And DPE molecules acted as bridges to connect H_4BDETP molecules. The unit cell was superimposed on the STM image and the measured parameters were: $a = 4.2 \pm 0.1$ nm, $b = 2.4 \pm 0.1$ nm, $\alpha = 88° \pm 1°$. The ratio of H_4BDETP to DPE was 2:1.

Different from H_4BDETP's self-assembly structure, H_4BDETP molecule in H_4BDETP/DPE lamellar structure (Fig. 2b) interacted with the adjacent face-to-face H_4BDETP molecule *via* a pair of O–H···O hydrogen bonds marked by black circle. Another carboxyl group of H_4BDETP molecule formed O–H···N with DPE molecule and O–H···O hydrogen bonds with the neighboring H_4BDETP molecule possessing the same orientation, which was indicated by yellow circle. And the remaining carboxyl groups of the H_4BDETP molecule were saturated by those of two adjacent H_4BDETP molecules. The energy per unit area of H_4BDETP/DPE structure (−0.296 kcal mol^{-1} Å^{-2}) displayed in Table S2 was lower than that of H_4BDETP's self-assembly structure (−0.260 kcal mol^{-1} Å^{-2}) [28], which supported the structural transformation of H_4BDETP's self-assembly system induced by DPE from a thermodynamic perspective, and agreed well with the experimental observation.

To investigate the regulatory effect of different bridging units in bipyridine on H_4BDETP's assembly structure, BPYB with a longer length was adopted. Unlike DPE, terminal pyridine groups in BPYB were connected by the biphenyl unit. In Fig. S3 (Supporting information), two kinds of H_4BDETP/BPYB lamellar structures were observed and marked as H_4BDETP/BPYB-I and H_4BDETP/BPYB-II respectively. In both types of lamellar structures, the ratio of H_4BDETP to BPYB was 1:1. In the high-resolution STM image of H_4BDETP/BPYB-I structure (Fig. 3a), H_4BDETP molecules (arched-shaped bright spots) with the same orientation were arranged into a column, and BPDYB molecules (bar-shaped bright spots) were inserted between two columns of the H_4BDETP distributed face-to-face. The measured lattice parameters were: $a = 5.8 \pm 0.1$ nm, $b = 2.4 \pm 0.1$ nm, $\alpha = 68° \pm 1°$. The calculated model (Fig. 3b) showed that two H_4BDETP molecules arranged into face-to-face were connected through O–H···N hydrogen bonds formed with two BPYB molecules, which could be taken as the building block. And each building block interacted with four adjacent

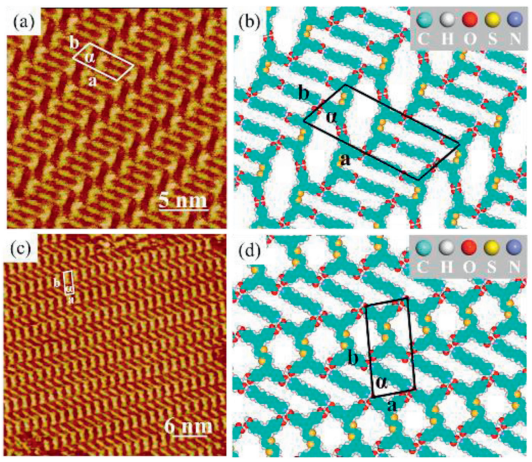


Fig. 3. High-resolution STM images of (a) H_4BDETP/BPYB-I and (c) H_4BDETP/BPYB-II co-assembly structures, the scanning conditions were: $I_{set} = 277.7$ pA, $V_{bias} = 690.0$ mV; $I_{set} = 277.7$ pA, $V_{bias} = 730.3$ mV. (b, d) The optimized molecular models for H_4BDETP/BPYB-I and H_4BDETP/BPYB-II co-assembly structures respectively. The insets in (b, d) indicated the blue atom was carbon, the white atom was hydrogen, the red atom was oxygen, the yellow atom was sulfur and the purple atom was nitrogen.

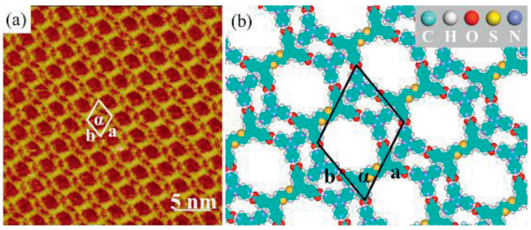


Fig. 4. (a) High-resolution STM image of H_4BDETP/TYPY co-assembly structure, the scanning conditions were: $I_{set} = 305.2$ pA, $V_{bias} = 676.6$ mV. (b) The calculated assembly model for H_4BDETP/TYPY co-assembly structure. The inset in (b) indicated the blue atom was carbon, the white atom was hydrogen, the red atom was oxygen, the yellow atom was sulfur and the purple atom was nitrogen.

ones through O–H···O hydrogen bonds between carboxyl groups of H_4BDETP.

Compared with H_4BDETP/BPYB-I structure, in H_4BDETP/ BPYB-II structure (Fig. 3c) H_4BDETP molecules appearing as H-shaped bright spots adsorbed on HOPG in a different configuration owing to the isomerism of sulfur atoms positions in thiophene groups. H_4BDETP and BPYB molecules were arranged alternately, which was similar to the co-assembly results of aromatic acids and pyridine in earlier reports [29,30]. The experimental lattice parameters were: $a = 1.6 \pm 0.1$ nm, $b = 3.6 \pm 0.1$ nm, $\alpha = 84° \pm 1°$. Fig. 3d showed that O–H···O hydrogen bonds existed between the neighboring H_4BDETP molecules along the direction of lattice parameter *a*, and O–H···N hydrogen bonds were formed between H_4BDETP and BPYB molecules in adjacent rows. In H_4BDETP/BPYB co-assembly system, the dimeric structure of H_4BDETP was completely disrupted by BPYB. Table S2 showed that total energies per unit area of H_4BDETP/BPYB co-assembly structures (−0.294, −0.296 kcal mol^{-1} Å^{-2}) were lower than that of H_4BDETP's mono-component structure, which was energetically beneficial for the formation of H_4BDETP/BPYB co-assembly structures.

Distinct from DPE and BPYB, the triazine core in TYPY was modified with three pyridine groups. Fig. S4 (Supporting information) showed H_4BDETP/TYPY structure differed from H_4BDETP's co-assembly structures with DPE or BPYB. It was seen from Fig. 4a that the dimeric structure of H_4BDETP was destroyed. Each H_4BDETP appearing as H-shaped bright spot was surrounded by six triangle bright spots representing TYPY molecules. Every two

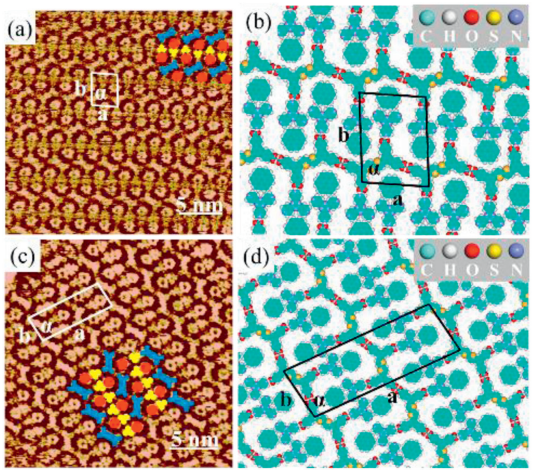


Fig. 5. High-resolution STM images of (a) H_4BDETP/TYPY/COR-I structure with the scanning conditions of $I_{set} = 280.8$ pA, $V_{bias} = 751$ mV, and (c) H_4BDETP/TYPY/COR-II structure with the scanning conditions of $I_{set} = 255.4$ pA, $V_{bias} = 751$ mV. (b, d) Optimized molecular models for the structures in (a) and (c) respectively. The insets in (b, d) indicated the blue atom was carbon, the white atom was hydrogen, the red atom was oxygen, the yellow atom was sulfur and the purple atom was nitrogen.

H_4BDETP molecules and two TYPY molecules formed a hexagonal nanopore. Along axis *b* direction, adjacent hexagonal nanopores shared one H_4BDETP molecule. The ratio of H_4BDETP to TYPY was 1:2 in the co-assembly structure. The experimental lattice parameters were: $a = 3.2 \pm 0.1$ nm, $b = 2.9 \pm 0.1$ nm, $\alpha = 69° \pm 1°$. According to the assembly model in Fig. 4b, the original O–H···O hydrogen bonds between H_4BDETP dimers were totally broken by TYPY. All carboxyl groups of H_4BDETP molecules formed new O–H···N hydrogen bonds with the pyridine groups of four TYPY molecules. And benzene rings of H_4BDETP molecule interacted with pyridine groups of another two TYPY molecules through C–H···N hydrogen bonds and π-π interactions.

When COR molecules were added to H_4BDETP/TYPY system, two kinds of multi-component co-assembly structures were formed (Fig. S5 in Supporting information). In these co-assembly structures, both the ratio of H_4BDETP to TYPY to COR was 1:2:2. High-resolution STM images (Fig. 5a and c) showed that COR could trigger the structural transformation of H_4BDETP/TYPY, and the subtle difference between two kinds of H_4BDETP/TYPY/COR structures lay in the arrangement of H_4BDETP molecules marked by blue H-shaped pattern. In H_4BDETP/TYPY/COR-I structure (Fig. 5a), two TYPY molecules with opposite orientations that were signed as yellow triangle pattern served as the bridge to connect neighboring H_4BDETP molecules along the direction of lattice parameter *b*. COR molecules labelled by red circular pattern entered the cavities surrounded by H_4BDETP and TYPY molecules. The experimental lattice parameters were: $a = 2.8 \pm 0.1$ nm, $b = 3.9 \pm 0.1$ nm, $\alpha = 95° \pm 1°$. The structural model (Fig. 5b) revealed that two carboxyl groups of each H_4BDETP molecule formed O–H···O hydrogen bonds with those of H_4BDETP molecules in the same row, and the remaining two carboxyl groups formed O–H···N hydrogen bonds with the pyridine groups of two TYPY molecules respectively. π-π interactions existed between the benzene rings of neighboring TYPY molecules. Each COR molecule was encapsulated by the cavity constituted by H_4BDETP and TYPY molecules, and formed π-π interaction with TYPY molecule. As shown in Figs. 5c and d, the intermolecular interactions in H_4BDETP/TYPY/COR-II structure were the same as those in H_4BDETP/TYPY/COR-I structure. Differently, H_4BDETP molecules in adjacent columns adsorbed on HOPG in two orientations, which led to the difference in the lattice parameters (Table S1). DFT results in Table S2 showed that the total energies per unit area of H_4BDETP/TYPY/COR assembly structures (−0.280, −0.273 kcal mol^{-1} Å^{-2}) were smaller than that of H_4BDETP/TYPY (−0.265 kcal mol^{-1} Å^{-2}), which indicated that H_4BDETP/TYPY/COR assembly structures were more energetically stable on HOPG.

In conclusion, H_4BDETP molecules self-assembled into linear structure in the form of hydrogen-bonded dimeric building blocks, which could be regulated by guest molecules. With the addition of COR, H_4BDETP transformed into nanoporous assembly structures to accommodate COR. H_4BDETP dimers in the H_4BDETP/COR-III structures were partially retained and formed new hydrogen bonds with H_4BDETP monomers, while all dimers in H_4BDETP/COR-I and II structures were destroyed. For pyridine derivatives, bipyridine molecules (DPE and BPYB) co-assembled with H_4BDETP into lamellar structures, while tripyridine molecules TYPY co-assembled with H_4BDETP into nanoporous structure owing to the increased binding sites brought by the additional pyridine group. And the difference in the central bridging unit between DPE and BPYB led to the discrepancy in their co-assembly structures with H_4BDETP. Besides, H_4BDETP/TYPY structure changed with the introduction of COR and two kinds of multi-component structures were obtained. This work may give insights into the regulatory behaviors of guest molecules on the self-assembly structures formed by hydrogen-bonded dimeric building block of aromatic acid derivatives.

Declaration of competing interests

The authors declare that they have no known competing financial interests or personal relationships that could have appeared to influence the work reported in this paper.

CRediT authorship contribution statement

Linlin Gan: Writing – original draft, Formal analysis, Data curation. **Xuan Peng:** Formal analysis, Data curation. **Wenchao Zhai:** Formal analysis, Data curation. **Cheng Zhang:** Software, Formal analysis, Data curation. **Xinyu Duan:** Formal analysis, Data curation. **Ke Deng:** Writing – review & editing, Software, Conceptualization. **Wei Li:** Writing – review & editing, Conceptualization. **Qingdao Zeng:** Writing – review & editing, Project administration, Funding acquisition, Conceptualization.

Acknowledgments

This work was financially supported by the National Natural Science Foundation of China (Nos. 22272039, 12064026), the Strategic Priority Research Program of the Chinese Academy of Sciences (No. XDB36000000), Natural Science Foundation of Jiangxi Province (No. 20232BABL201036) and the Jilin Chinese Academy of Sciences-Yanshen Technology Co., Ltd.

Supplementary materials

Supplementary material associated with this article can be found, in the online version, at doi:10.1016/j.cclet.2024.110667.

References

[1] K. Thorkelsson, P. Bai, T. Xu, Nano Today 10 (2015) 48–66.
[2] S. Chagri, D.Y. Ng, T. Weil, Nat. Rev. Chem. 6 (2022) 320–338.
[3] D.D. La, H.H. Ngo, D.D. Nguyen, et al., Coordin. Chem. Rev. 463 (2022) 214543.
[4] L. Grossmann, E. Ringel, A. Rastgoo-Lahrood, et al., Angew. Chem. Int. Ed. 61 (2022) e202201044.
[5] K. Gurdumov, U. Mazur, K. Hipps, J. Phys. Chem. C 126 (2022) 12916–12927.
[6] J. Ren, M. Freitag, Y. Gao, et al., Angew. Chem. Int. Ed. 61 (2022) e202115104.
[7] X. Wang, Y.Q. Wang, Y.C. Feng, et al., Chem. Soc. Rev. 50 (2021) 5832–5849.
[8] S. Sun, B. Li, W. Xiong, et al., Appl. Surf. Sci. 636 (2023) 157769.
[9] J. Teyssandier, S. De Feyter, K.S. Mali, Chem. Commun. 52 (2016) 11465–11487.
[10] S. Zhang, L. Cheng, C. Chen, et al., Langmuir 37 (2021) 2153–2160.
[11] S.B. Khan, S.L. Lee, Molecules 26 (2021) 3995.

[12] C. Ma, J. Li, S. Zhang, et al., J. Phys. Chem. C 124 (2020) 23237–23242.
[13] X. Peng, Y. Geng, M. Zhang, et al., Nano Res. 12 (2019) 537–542.
[14] X. Li, J. Li, C. Ma, et al., Chin. Chem. Lett. 32 (2021) 1077–1080.
[15] R. Xie, X. Zeng, Z.H. Jiang, et al., Langmuir 39 (2023) 3637–3644.
[16] S. Wang, P. Lei, Z. Huang, et al., Langmuir 40 (2024) 18999–19007.
[17] K. Gurdumov, U. Mazur, K. Hipps, J. Phys. Chem. C 126 (2022) 19904–19915.
[18] Y. Zheng, S. Zhang, X. Zhao, et al., Langmuir 40 (2024) 6424–6431.
[19] P. Lei, W. Luo, K. Deng, et al., New J. Chem. 47 (2023) 18010–18017.
[20] Y. Liu, X. Zhao, S. Zhang, et al., Chin. Chem. Lett. 35 (2024) 109404.
[21] L. Ma, P. Wang, W. Duan, et al., Langmuir 37 (2021) 11544–11551.
[22] H. Pinfold, C. Greenland, G. Pattison, et al., Chem. Commun. 56 (2020) 125–128.
[23] Y. Hong, L. Wang, S.F. Wang, et al., CrystEngComm 23 (2021) 3849–3855.
[24] F. Cometto, K. Frank, B. Stel, et al., Chem. Commun. 53 (2017) 11430–11432.
[25] J. Li, B. Liu, W. Duan, et al., Surf. Sci. 700 (2020) 121654.
[26] S. Zhang, C. Chen, J. Li, et al., Nanoscale 14 (2022) 2419–2426.
[27] P. Lei, L. Ma, S. Zhang, et al., Chin. Chem. Lett. 34 (2023) 108005.
[28] X. Peng, L. Gan, W. Zhai, et al., Nanoscale Adv. 5 (2023) 4752–4757.
[29] X. Peng, L. Cheng, X. Zhu, et al., Nano Res. 11 (2018) 5823–5834.
[30] T. Meng, P. Lei, Y. Zhang, et al., Chin. J. Chem. 40 (2022) 2727–2733.